Information flow between interacting human brains: Identification, validation, and relationship to social expertise

Edda Bilek[a,1], Matthias Ruf[b,1], Axel Schäfer[a], Ceren Akdeniz[a], Vince D. Calhoun[c,d], Christian Schmahl[e], Charmaine Demanuele[a], Heike Tost[a], Peter Kirsch[f,1], and Andreas Meyer-Lindenberg[a,1,2]

Departments of [a]Psychiatry and Psychotherapy, [b]Neuroimaging, [e]Psychosomatic Medicine and Psychotherapy, and [f]Clinical Psychology, Central Institute of Mental Health, Medical Faculty Mannheim, Heidelberg University, 68159 Mannheim, Germany; [c]Mind Research Network, Albuquerque, NM 87131; and [d]Department of Electrical and Computer Engineering, University of New Mexico, Albuquerque, NM 87131

Edited by David M. Eagleman, Baylor College of Medicine, Houston, TX, and accepted by the Editorial Board March 13, 2015 (received for review November 14, 2014)

Social interactions are fundamental for human behavior, but the quantification of their neural underpinnings remains challenging. Here, we used hyperscanning functional MRI (fMRI) to study information flow between brains of human dyads during real-time social interaction in a joint attention paradigm. In a hardware setup enabling immersive audiovisual interaction of subjects in linked fMRI scanners, we characterize cross-brain connectivity components that are unique to interacting individuals, identifying information flow between the sender's and receiver's temporoparietal junction. We replicate these findings in an independent sample and validate our methods by demonstrating that cross-brain connectivity relates to a key real-world measure of social behavior. Together, our findings support a central role of human-specific cortical areas in the brain dynamics of dyadic interactions and provide an approach for the noninvasive examination of the neural basis of healthy and disturbed human social behavior with minimal a priori assumptions.

fMRI | hyperscanning | joint attention

Human social interactions have likely shaped brain evolution and are critical for development, health, and society. Defining their neural underpinnings is a key goal of social neuroscience. Interacting dyads, the simplest and fundamental form of human interaction, have been examined with behavioral setups that used real movement interactions during communication in real time as a proxy (1–4), providing mathematical models representing human interaction, goal sharing, mutual engagement, and coordination. To identify the neural systems supporting these behaviors, neuroimaging would be the tool of choice, but studying dyadic interactions with this method is both experimentally and analytically challenging. Consequently, the neural processes underlying human social interactions remain incompletely understood.

Experimentally, studying dyads with neuroimaging technology that allows only one participant per scanner provides challenges that have been addressed in the literature in one of two ways. First, the audiovisual experiences of human social contact have been simulated using stimuli such as photographs, recorded videos, or computerized avatars in the absence of human interaction (5–7), or, recently, immersive audiovisual linkups have been used with one of the two participants being scanned (8, 9). Secondly, pioneering neuroimaging experiments have coupled two scanner sites over the Internet, a setup called hyperscanning, enabling subjects to observe higher-level behavioral responses such as choices made to accept or reject an offer in real time while in the scanners (10, 11). In the current study, we aimed to combine the advantages of these experimental approaches by enabling two humans to see (and possibly hear) each other in a hyperscanning framework, enabling an immersive social interaction while both participant's brains are imaged. To do so, we implemented a setup with delay-free data transmission and precisely synchronized data acquisition, in addition to a live video stream provided between scanner sites during the entire session (Fig. 1*A*). While real-time video transmission is not an indispensable requirement for the study of all forms of social interaction, it is a naturalistic presentation method for visual social stimuli in the scanner, and likely helpful for the study of interactions involving changes in eye gaze and facial expressions, although the advantages of the precise temporal synchronization are partially mitigated by the low temporal resolution of the blood oxygen level-dependent (BOLD) response and the sampling frequency of functional MRI (fMRI) experiments.

Analytically, extracting and testing for information flow in the resulting joint neuroimaging data are not straightforward. In this paper, we describe a general analysis framework for this problem that makes only minimal a priori assumptions. Importantly, using permutation testing, we also aim to address the open question of whether there is anything neurally specific or even unique about

Significance

Social interaction is the likely driver of human brain evolution, critical for health, and underlies phenomena as varied as childhood development, stock market behavior, and much of what is studied in the humanities. However, appropriate experimental methods to study the underlying brain processes are still developing and technically challenging. Here, we extend previous pioneering approaches in neuroimaging [functional MRI (fMRI) hyperscanning] to provide a method for studying information flow between interacting humans in a two-person approach. A scan environment enabling synchronized data acquisition and interaction-based fMRI tasks is described. We provide a generally applicable analysis method to identify interacting brain systems. Specific social brain systems are identified as drivers of interaction in humans, and we find a link to a measure of social expertise.

Author contributions: E.B., P.K., and A.M.-L. designed research; E.B., M.R., and C.A. performed research; E.B., A.S., V.D.C., C.D., H.T., and A.M.-L. analyzed data; E.B., M.R., A.S., C.A., V.D.C., C.S., H.T., P.K., and A.M.-L. wrote the paper; and M.R. built the required hardware.

A.M.-L. has received consultant fees and travel expenses from Alexza Pharmaceuticals, AstraZeneca, Bristol-Myers Squibb, Defined Health, Decision Resources, Desitin Arzneimittel, Elsevier, F. Hoffmann-La Roche, Gerson Lehrman Group, Grupo Ferrer, Les Laboratoires Servier, Lilly Deutschland, Lundbeck Foundation, Outcome Sciences, Outcome Europe, PriceSpective, and Roche Pharma and has received speaker's fees from Abbott, AstraZeneca, BASF, Bristol-Myers Squibb, GlaxoSmithKline, Janssen-Cilag, Lundbeck, Pfizer Pharma, and Servier Deutschland.

This article is a PNAS Direct Submission. D.M.E. is a guest editor invited by the Editorial Board.

[1]E.B., M.R., P.K., and A.M.-L. contributed equally to this work.

[2]To whom correspondence should be addressed. Email: a.meyer-lindenberg@zi-mannheim.de.

This article contains supporting information online at www.pnas.org/lookup/suppl/doi:10.1073/pnas.1421831112/-/DCSupplemental.

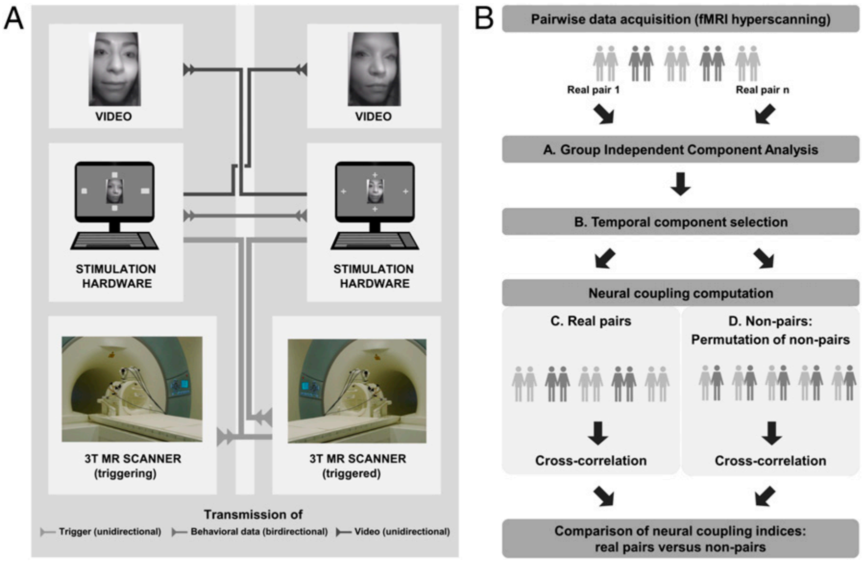

Fig. 1. Hardware environment and analysis routine for fMRI hyperscanning. (*A*) Illustration of the hyperscanning setup as implemented for the present studies. (*B*) Schematic overview of the analysis routine for the examination of information flow between interacting human brain systems in hyperscanned fMRI data. Letters correspond to the numbering of in-text analysis steps.

human dyadic interaction, compared with a situation in which no real-time information is exchanged.

In the current paper, we study joint attention (JA), a basic yet fundamental mechanism of social interaction that is used by humans to coordinate and communicate intentions and information as well as guiding others' attention in a nonverbal way, especially through eye gaze (12). JA is of considerable interest both for cognitive and clinical neuroscience because it arises early in development, preceding and shaping the emergence of symbolic communication and higher-order social functions such as representational theory of mind (13, 14). Disturbances of JA in developmental disorders with prominent social disturbances such as autism and attention deficit hyperactivity disorder, but also schizophrenia, have been identified (see, e.g., refs. 13 and 15).

To investigate JA, we used a paradigm where information on a target location is given to one subject (sender of information) only, but both subjects (sender and receiver) must respond correctly by indicating the target location on a button response device. Thus, information needs to be transferred from one subject to another nonverbally while fMRI data are acquired, resulting in flow of information between two interacting brain systems (interaction phase, INT). For determination of interaction-based aspects of the fMRI data, control phases without interaction were added to the task protocol (NoINT). We studied a discovery sample to identify the main neural parameters of information flow ($n = 26$) and, for confirmation, a larger independent replication sample ($n = 50$). Combined, these data were used to validate the approach and relate the resulting parameters to socially relevant psychometric measures. Based on the previous literature on neuroimaging in JA, we expected that we would see information flow involving the temporoparietal junction and medial prefrontal cortex. However, to keep methodological assumptions in this new field minimal, we decided to not include this as an a priori hypothesis into our analysis.

Results

Analysis Summary. To characterize information flow between interacting brains, we used a data-driven approach with minimal assumptions. In brief, we extracted components (spatiotemporal summaries of brain activity) from all participants' data (step A), selected brain components active during interaction in individual brains (step B), estimated the information flow between components in interacting pairs (step C), and used randomization to demonstrate that coupling is unique to interacting pairs (step D) (Fig. 1*B*). A detailed description of all analysis steps is provided in *Methods*.

Discovery Study. In a first analysis step requiring minimal prior assumptions on data characteristics, we applied a multivariate group independent component analysis (ICA) (16–19) to the data of 26 healthy subjects (13 pairs) in step A. This data-driven approach identified 16 maximally independent sources (components) that, together, account for the observed fMRI data of all subjects (Fig. S1). Of these, one noise component (defined as predominantly extracerebral signal) was removed.

In step B, components relevant for social interaction (component of interest, COI) were identified. COIs should, by definition, be significantly more active while subjects are interacting. Thus, we computed temporal association indices for each component and task phase of interaction, as well as phases of no interaction (multiple regression analysis); i.e., a parameter for each subject, for a given component, within each task block, and to each phase of the task, reflecting the overall temporal association of the component with the respective task phase. Subsequently, all components that did not exhibit a significantly higher association with INT were excluded. After this step, six components were identified as COIs (repeated measures ANOVA; all $F > 6.9$, $P < 0.02$, Table S1).

In step C, to map the information flow from one brain to another, we computed cross-correlations between COI for each COI pair (i.e., each COI extracted from sender with each COI extracted from receiver). Computations included estimations of the optimal time shift (lag) (11, 20, 21), indicative of the transfer time between neural systems.

Finally, in step D, to investigate whether hyperscanning data captured the flow of information between interacting subjects, we tested whether the coupling between COI systems was significantly different from that in pairs that performed the identical task protocol, but were not actually interacting with each other. For this, we recombined data from these real pairs to form nonpairs (e.g., sender pair A/receiver pair B), and repeated step C analysis. Neural coupling indices for each lag of real pairs and nonpairs were then compared [permutation-based tests, corrected for multiple comparisons using false discovery rate (FDR)]. This revealed that two COI pairs showed significantly higher neural coupling in real pairs relative to nonpairs within a time window of 0–1.55 s ($P_{FDR} < 0.04$; Table S2).

Notably, both identified pairs had the same neural system in the sender, a component spatially comprising the right temporoparietal junction (rTPJ, component 11, Fig. 2*A*). Neural coupling of the sender's rTPJ with the receiver's rTPJ was found to be unique to real pairs in the discovery study data; additionally, neural coupling was found between the sender's rTPJ and a COI spatially highly associated with prefrontal regions, medial prefrontal cortex (mPFC), and orbitofrontal cortex, respectively (component 13, Fig. S1).

Replication Study. To gain further confidence in the initial findings, the study was repeated in a larger, independent sample of 50 healthy subjects (25 pairs), and the analysis routine was applied as described above. Step A group ICA (GICA) identified 16 maximally independent components from the concatenated data, the same number as estimated for the discovery study data (Fig. S2). Within step B, six components exhibited relevant temporal properties and were included as COI (positive association with INT that is significantly higher than the association with NoINT, all $F > 8.6$, $P < 0.002$; Table S1).

Following results derived from the discovery data, COIs were screened for spatial consistency with component 11 of the discovery data; i.e., the COI covering rTPJ was identified (Table S3 and Fig. 2*B*). Neural coupling indices were computed as specified in step C between the sender's rTPJ component and all identified COIs. Lastly, nonpair data were created by permutation of real pairs (step D). This confirmed the initially found synchronization of the sender's and receiver's rTPJ as unique to interacting subjects ($P_{FDR} = 0.001$, Table S4). Coupling between the sender's rTPJ and prefrontal regions was not confirmed in the replication data.

Relationship to Social Expertise. Finally, to examine evidence for the behavioral relevance of our findings, we tested whether coupling indices are associated with parameters of the subject's social functioning, as indexed by the average complexity of a pair's social networks. The self-report questionnaire social network index (SNI) (22) is a repeatedly used measure describing the complexity and size of the social network a subject is embedded in, and has been found to be related to neural markers such as the volume and function of socially relevant brain regions (23–26). Indeed, the coupling index proved to be significantly positively associated with the mean social network complexity of real pairs (repeated measures ANOVA; $F = 5.0$, $P = 0.03$). Thus, dyads living in more-complex social networks (i.e., pairs having regular contact with individuals from a greater variety of social groups, such as family, coworkers, sports peers, religious peers) displayed stronger between-pair neural coupling during JA interaction.

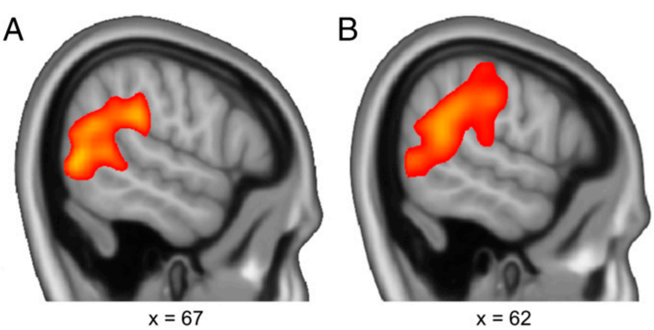

Fig. 2. ICA components showing neural coupling only in interacting subjects typically cover the right TPJ. (*A*) Component 11 (discovery study). (*B*) Component 5 (replication study). See Figs. S1 and S2 for display of both full sets of components.

Discussion

In the present work, we aimed to develop a neuroimaging approach enabling us to identify neural systems in interacting human dyads with minimal a priori assumptions. A coupled neural system centered at a key region for social interaction, rTPJ, was identified in this process and confirmed in a replication experiment.

TPJ is a supramodal association area integrating input from thalamus, visual, auditory, somaesthetic, and limbic areas of the cortex. Specifically, the rTPJ has been implicated in two sets of functions, both of which are relevant to JA: reorienting of attention and social cognitive functions ranging from the processing of socially relevant motion and cues, to inferring social intentions, to a representational theory of mind (27–30). Importantly, both functional domains not only depend on rTPJ but are also developmental prerequisites of JA and therefore a functional basis of higher-order social cognitive functions. Recently, a functional segmentation of rTPJ was suggested, with anterior rTPJ being relevant both for attention shifting and processing of social information, while posterior rTPJ is concerned with theory of mind (31). The full structure would then serve as an integrating core for mentalizing, and judging/planning of social behavior (31–33). The ICA components observed as coupled during social interaction in our study cover both anterior and posterior rTPJ. Consequently, we consider it plausible that, in line with the integration of social information and the central role in forming social behavior, rTPJ function is the basis of unique neural synchrony in interacting subjects. In agreement with this, previous experiments invoking JA with one participant being scanned have shown right-sided activation of TPJ or posterior superior temporal sulcus (8, 9, 34, 35).

The social cognitive relevance of the observed cross-brain coupling originating from rTPJ is further supported by our finding that, in the discovery sample, the second significantly coupled dyad linked rTPJ to prefrontal cortex, especially mPFC. This latter brain region has been proposed, together with rTPJ, as supporting uniquely human social cognition (36). Specifically, dorsal mPFC is implicated in the uniquely human representation of triadic relations between two minds and an object, supporting JA, and has been observed in single-participant JA experiments (37), and in a dual-participant JA experiment with one subject in the scanner (9, 35). However, our observation was not replicated in the second sample we studied and must therefore be considered preliminary until followed up by larger studies using a hyperscanning framework.

Significant differences in neural coupling were observable within a delay time bin between the neural signals of 0 s to ~3 s, which is a plausible time frame necessary for the information to be transferred and processed between brains. In two independent samples, we showed that temporal coupling was significantly linked to interaction of a pair: Neither synchronized task performance that did not require interaction (NoINT phases) nor interaction with any partner but the real one (nonpairs) produced similar synchronized brain activity. Nevertheless, the time resolution of fMRI, which is limited by the temporal course of the BOLD response and the ability to sample it in imaging, likely captures the underlying dynamics of the pair interaction only incompletely; we speculate that coupling strength in the dyad may wax and wane across the time course of a trial. In a supplementary analysis, we examined whether differences in coupling of interacting pairs extended into later time periods and did indeed find significant increases also in later time periods (*SI Text, Increase of Neural Coupling over Time*), which argues that periods of synchronized activity persist and/or recur later in the dyadic interaction.

Because the goal of this paper was to identify neural coupling measures in direct social interaction, we hypothesized that these signatures would be related to real-world social functioning. Based on previous studies, we chose the complexity of the social environment (22), which had been found to be related to connectivity strength within social brain networks in humans as well as to the size of a main subregion, the amygdala (23, 26). Indeed, we found a relationship in the expected direction, with higher coupling related to increasing real-world social complexity. Interestingly, neuroimaging data in macaques have shown that activity of superior temporal sulcus, a potentially homologous area to TPJ, was linked to social network size, pointing to an evolutionarily conserved or elaborated mechanism (38).

Our study has several limitations. First, because our focus was on identifying information flow between interacting dyads with as few assumptions as possible, but stringent statistical testing, the approach taken in this paper is conservative. It is conceivable that additional interacting systems can be identified as two-person neuroscience advances and more knowledge about the relevant systems can be assumed a priori. Second, as stated, the time resolution of fMRI is likely not able to characterize interaction events fully, calling for future methodological advances in joint EEG–fMRI hyperscanning. Third, because we chose JA as a simple yet fundamental mechanism of social interaction, this led to results in behavioral data at-ceiling, which could therefore not be associated with the magnitude of neural coupling. More complex tasks should, in the future, permit a direct study of the relationship between on-task performance and coupling. Fourth, future studies may consider the use of alternative control conditions. Although our approach aimed for a comparable perceptual stimulation, other control scenarios may include the extraction of directional information from a nonsocial object (e.g., an arrow in the center of the display indicating where to look) or the presentation of a recorded (noninteracting) video of a partner. Finally, our replication sample consisted only of female dyads; gender effects in coupling should be studied in the future.

In conclusion, we implemented a hyperscanning environment to study the neural mechanisms of dyadic social interaction in humans, overcoming some prior research constraints. We developed a generally applicable analysis method with minimal a priori assumptions, identified neural coupling that is unique to interacting pairs and specific involvement of rTPJ, replicated our findings, and validated them by associating the derived parameters of brain interaction with a psychometric measure of social expertise. We hope that the outlined experimental approach will be useful to further study the neurobiological underpinnings of human dyadic social interaction, a core interest of both basic social and clinical neuroscience. Most common psychiatric disorders impair social behavior, and, conversely, social interactions in psychotherapy are a mainstay of treatment. Current knowledge of the underlying biological mechanisms is minimal, and can be advanced by two-person neuroscience approaches such as the one described here.

Subsequent studies could examine the psychiatric and biological involvement of neural coupling. In addition to complex interaction, clinical samples with known impairment in social behavior or neurobiological interventions such as transcranial magnetic stimulation should be considered to evaluate sensitivity and specificity of this parameter and rTPJ function. Finally, the ability to identify linked systems across brains will inform neuroscience research on phenomena such as social hierarchy, defeat, trust, attraction, and other key questions in which the examination of natural immersive human interactions is a significant methodological advancement.

Methods

Hyperscanning Environment. To create an immersive hyperscanning environment, two identical 3 Tesla MRI scanners, located ~100 m apart, were directly connected via optical fibers (duplex fiber, straight tip fiber optic connector, 62.5 μm/125 μm; outlined by Fig. 1*A*). Identical scanners are relevant, because signal differences between varying platforms may overshadow meaningful effects of task or social interaction in fMRI data (a brief discussion of recommendations is given below). Also, using direct connections of fiber optics instead of Ethernet and Internet protocols enabled the exchange of signals between scanner sites in real time (data transmission delay < 1.5 μs), which is essential for scanner and fMRI hardware synchronization and optimal quality of the live video transmission. Fiber optics were used for transmission of scan trigger signals, video streams, and behavioral data. For fMRI synchronization, the optical trigger signal from one scanner was sent to the other, where it initiated fMRI image acquisition and also served to synchronize the task-related software with data acquisition (approximately every 10 s). For recording of high-quality facial visual stimuli, which is essential for a naturalistic social interaction experience, a mirror box was custom made by MRC Systems GmbH to fit a 12-channel-MR head coil and hold two MR-compatible cameras along with the respective light sources. IR light was chosen to avoid distracting visible illumination in the subjects' sight. One camera, used in the study reported here, captured the entire subject's face image in a focal width of 3.6 mm, an image sensor format of 1/3 inch, and recording at a frame rate of 50 Hz (model MR_CAM Hyper-Scanning); a second camera was mounted, suitable to provide eye-tracking images in future studies. The cameras were placed behind a 45° tilted one-way mirror, thus unseen by the subject. The live image of the camera was transmitted to the other scan site, where it was merged with the stimulus display, a 40-inch liquid-crystal display at the head end of the MRI scanner. Audio contact was not provided in this study. The scan protocol was identical at both sites.

Hardware Setup for Hyperscanning Studies.

Connection of scanner sites. Use of Internet-based Transmission Control Protocol/Internet Protocol for the connection of scanner sites (10), while enabling long-distance connection of research laboratories, brings about an unpredictable amount of delay, depending on the location and number (hop count) of router/gateways that data are transferred across before reaching the actual destination (round trip times of up to 300 ms, depending on server location). However, for signal bursts to be interpreted correctly by our stimulation devices (Presentation: Neurobehavioral Systems; see www.neurobs.com/index_html), temporal jitter due to the round trip time of transmitted data packages cannot be larger than 40 ms. Thus, to create an environment that enables precise synchronization of scanners and stimulus presentations, we chose a direct connection of scanner sites via fiber optics. Although the neural readout (BOLD response) evolves over seconds, as do many forms of social interaction, some aspects of social communication, such as eye gaze and facial expressions, operate on a much shorter time scale. This makes the lag-free video and response transmission of the hyperscanning environment particularly suitable for the study of these (but not all) forms of human interaction, even though the advantage of the precise synchronization is partially mitigated by the time scales of the BOLD response and the sampling frequency of whole-brain fMRI acquisitions.

Identical MRI scanner types. To eliminate important sources of noise, we equipped our scanner sites with fully identical hardware. Otherwise, between-scanner variance from nonidentical sites is induced in the data and is confounded with the effect of interest in hyperscanning studies; the same likely applies for different scanner types. For example, Takao et al. (39) reported significant differences in brain volume measured by identical scanner sites, and other studies suggest rather large differences in data acquired on different scanner vendors and/or field strengths that should be considered in the design of multisite studies (40, 41). For functional data, differences of signal detection at 1.5 T versus 3 T have been reported (42), and Friedman et al. (43) found poor reliability of multisite (field strength and vendor) data acquisition, proposing multiple factors to improve comparability, e.g., selection of large regions of interest or averaging multiple runs, both not practicable solutions for hyperscanning. Although these studies do not support a final conclusion, they point to a plausible bias of hyperscanning data that increases with differences in the acquisition hardware. We thus recommend keeping setups as similar as possible, although the minimization of interscanner variability may bias the approach toward the idiosyncracies of a specific scanner. This implies that the suggested homogeneity of setups may involve a trade-off between reduction of confounds and generalizability of results.

Subjects. Two independent samples of right-handed healthy volunteers were successively recruited from the population of the city of Mannheim, Germany. Thirty subjects participated in the discovery study, and, following its completion, a second sample of 56 healthy volunteers was independently recruited for replication. All participants provided written informed consent for a protocol approved by the Ethics Committee of the University of Heidelberg and were screened before inclusion for the absence of a lifetime history of psychiatric or neurological illness, pregnancy, a history of head trauma, and current alcohol or drug abuse. Subjects were randomly assigned to same-sex dyadic pairs and scanners. Five pairs (10 subjects) had to be excluded after data inspection (one due to incomplete fMRI data of one subject; two because of excessive head movement during data acquisition; two due to insufficient task performance, i.e., not indicating the target position by eye gaze). A sample of 26 subjects formed the discovery group (10 males, mean age = 24.5 ± 4.6 y, mean education = 12.8 ± 1.2 y), and 50 subjects were included in the replication sample (all female, mean age = 23.4 ± 3.3 y, mean education = 12.6 ± 1.3 y).

Task. The task combined phases of interaction (INT) between the subjects and phases of individual performance (NoINT), as well as feedback. During INT, subjects had to press a target button on an MR-compatible response device that corresponded to the location of target shapes on the stimulus presentation screen (i.e., left, right, bottom, or top). The target shape (square) was shown randomly at one of the four positions across trials, and distractor shapes (e.g., parallelogram, rectangle) were assigned to the remaining positions (see Fig. S3*A* for examples). A successful trial required both subjects to press the same target button, although the target shape was presented to one subject (i.e., the "sender" of information) only. Stimuli in the shape of a plus sign (equal in size and similar in complexity to the target and distractor shapes) were shown to the other subject (i.e., the "receiver" of information, Fig. S3*B*). The receiver was therefore dependent on the information given by the sender about the target position. To gain this information, receivers were instructed to locate the target by following the sender's eye gaze; the sender, in return, marked the target location by a gaze shift in the corresponding direction. Hence, a successful trial required cooperation and information flow between sender and receiver. To isolate the interaction-based aspects of the fMRI data, phases of comparable perceptual stimulation without interaction were added to the task protocol. During NoINT, the same stimulus configuration presented to the sender in the interaction condition was presented to both subjects (one target, three distractors, fixed positions; same target position, random distractor shapes), so that no cooperation was necessary to successfully complete the trial. Subjects were instructed to solve the NoINT condition independent of their partner, and senders were not instructed to perform voluntary eye movement.

The full task included two scan blocks of 40 trials (alternating phases 40 × INT, 40 × NoINT; 5 s each), followed by a performance feedback (3 s). Task roles (sender/receiver) were switched after the first half of trials, so that each subject performed both task roles across the measurement either in the first or the second half (block A or block B). Including a break between blocks for instruction of subjects for role switch, buffering scans for device synchronization, and a temporal jitter between trials to vary stimulus presentation onsets, total task time summarized to 598 s in the discovery study and 645 s in the replication study, for which an extended jittering delay was used. Live video transmission was provided continuously over the entire task. The video image was centered on screen, and task stimuli were arranged at the respective positions around the video image.

Data Acquisition and Preprocessing. Data were acquired on both scanners, applying parallel imaging to improve temporal resolution (TR) of data, and with the following parameters: TR = 1550 ms, TE = 30 ms, FOV = 192 mm^2, 28 slices, 4-mm thickness, 1-mm gap, flip angle 73°, 393/390 volumes (discovery study) or 423/420 volumes (replication study). For the following analysis steps, a conventional preprocessing routine was applied using Statistical Parametric Mapping software (SPM8, www.fil.ion.ucl.ac.uk/spm/software/spm8/) in MATLAB (version 2011b, www.mathworks.com/products/matlab/). Data were realigned to mean image, slice time corrected, normalized to standard stereotactic space (as defined by the Montreal Neurological Institute), and smoothed using a Gaussian kernel filter with 8-mm FWHM.

Analysis Step A: ICA. ICA is a data-driven blind source separation approach, which extracts the underlying, maximally independent sources (components) from a multivariate data set. GICA was conducted using the GIFT toolbox for MATLAB (GIFT version 2.0e, mialab.mrn.org/software/gift/). Here, a spatial ICA is performed [INFOMAX algorithm (44)], while subject data are temporally concatenated in one aggregate data matrix X to obtain grouped spatial maps valid for the whole sample in

$$X = G^{-1}\begin{bmatrix} F_1^{-1} & Y_1 \\ F_N^{-1} & Y_N \end{bmatrix}$$

where F_i^{-1} and G^{-1} are subject and group reduction matrices [as determined by principal component analysis (PCA)], respectively, and Y_i is the data matrix. Furthermore, subject-specific time courses of each component are available via back reconstruction, for which the partitioned data reduction matrices are projected to aggregate component matrix [components in rows; used back reconstruction algorithm GICA I (16, 17, 18)]. This is called PCA-based back reconstruction and was shown to be highly accurate compared with other approaches to back reconstruction (17). Because task-related roles are switched after the first half of the paradigm, subject data were entered with task blocks (block A and block B) as separate sessions to enable us to model the task role-specific differences. For GICA, the dimensionality of the data (i.e., number of components to be estimated) can be assessed, among other estimation methods, by computing the minimum description length for each subject's dataset (16); this was found to be 16 in both reported data sets. To assure a reliable estimation of components, GICA was repeated and estimations were compared by using ICASSO software (17, 45) (research.ics.aalto.fi/ica/icasso/). Component spatial maps were scaled to percent signal change for more convenient comparison and interpretation, and all other analysis settings were applied as commonly reported for the procedure (16, 19). Components were assigned consecutive numbers for identification, although the assigned numbers are arbitrary because components are not sorted in any way by ICA.

Notably, the group-based ICA approach described here results in spatial components for the entire sample, which allows for comparisons of individual temporal data. An interesting alternative approach for future studies is dyad-based blind source separation. Although the comparability of components across dyads may be limited, this approach has the prospect of informing the field on differences in interdyadic neural processing.

Analysis Step B: Temporal Component Selection. Multiple regression analysis was performed on the task design as a dependent measure using the subject-specific mean temporal data for each component as explanatory variables. This results in a subject-specific beta value for INT as well as NoINT, both separate for two task blocks. Beta values from the discovery study were found to be uncorrelated for different blocks (coding for task roles) in all but three components, pointing to role-specific brain activity within subjects (mean Spearman rank correlation of blocks A and B $r = 0.02$). A stable correlation across phases was exclusively found for component 3, that is, a component covering solely the primary visual cortex and processing relatively similar stimuli sets across subjects, trials, and task roles (INT were correlated across blocks in a component capturing movement artifacts; NoINT were correlated in a component covering the cuneus and inferior parts of the precuneus across the parietal–occipital fissure).

Next, standardized (z-scored) beta values for each subject were entered in a repeated measures ANOVA with task phase and block as within-subject factors to exclude all components not showing a significantly higher association with INT over NoINT, while accounting for additional within-subject dependency (for each subject, four parameters were estimated: two phases in block A and two phases in block B). This procedure, applied to discovery study data, identified 10 components showing a significant difference in the degree of association with defined task phases. Further inspection of the remaining component set revealed that one component was significantly more highly associated with NoINT and was therefore excluded from the analysis, while 3 of the 10 associated components did exhibit a negative beta weight for INT (Table S1). Considering a negative beta weight as a measure of deactivation during the respective task phase, we believe these components can be potentially meaningful for certain hypotheses (i.e., deactivation of an inhibitory control region under task demand might indicate disinhibition within networks). However, aiming to identify information flow across brains that would appear as an active representation at the neural level, deactivated brain regions were not considered for further analyses.

Similar results were obtained for the replication sample data. Here, a significant difference in temporal association with task phases was found for 12 out of 16 components. Furthermore, one component was significantly more highly associated with NoINT, and negative beta values for INT were observed for five components of this set, resulting in six components to be considered for spatial component selection (Table S1).

Analysis Step C: Lag Estimation. Investigating the extent of neural coupling within simultaneously scanned subjects, component time courses were back-reconstructed to obtain the individual subject's time course corresponding to each spatial map. Cross-correlation was computed as a measure of neural coupling, in which each pair's time courses in a given COI pair in the discovery sample data were correlated (e.g., COI1 from sender and COI2 from receiver); this was done repeatedly across all possible combinations of COIs (COI1 through COI6 from sender and COI1 through COI6 from receiver, 36 component pairs in total).

As previous reports suggest, neural coupling computations may need to take into account a temporal delay required for the flow of information between brain systems (11, 20, 21). For this, the receiver's time course was repeatedly shifted by one TR (one lag) forward in time, and correlated again, until, after nine lag shifts, the end of one trial was reached. Time series were shifted unidirectionally only, corresponding to the direction of information flow, with the sender's time course leading the receiver's time course (i.e., considering the sender's time course fixed, the receiver's time course was shifted forward in time). Because task design included a role switch after the first half of the experiment, lag estimation was computed twice for each couple (block A with

NEUROSCIENCE

subject N_i as sender, block B with subject N_i as receiver). Full lag estimated data therefore consisted of neural coupling indices for each couple, at each lag, and in each of the investigated COI pairs.

Analysis Step D: Permutation-Based Tests. For each COI, we used a nonparametric permutation-based approach to compare the coupling indices of really interacting pairs (i.e., interacting individuals that were scanned simultaneously, e.g., the sender and receiver of pair A) to those of randomly composed nonpairs. The nonpairs were created by matching individuals to partners other those they had performed the task with (e.g., by matching the sender of pair B to the receiver of pair C).

For the discovery sample, the reference distribution of nonpairs was created by 1,000 repetitions of the artificial sender/receiver pair assignments. During each repetition, a random sample of 26 nonpairs ($\triangleq 13 \times 2$ real pairs) was drawn from the distribution of permutated nonpairs, and lag estimation was conducted as described above. For the replication sample, permutation was repeated 10,000 times, and random samples of 50 nonpairs ($\triangleq 25 \times 2$ real pairs) were drawn. Next, the frequency of $\text{correlation}_{\text{NON-PAIRS}} > \text{correlation}_{\text{REAL PAIRS}}$ was determined (i.e., the ratio of (*i*) the number of cases in which real pairs did not show higher neural coupling than nonpairs and (*ii*) the number of total observations, i.e., 1,000 or 10,000). This frequency represents the empirical *P* value testing whether neural coupling occurred that is unique to real pairs. To determine the time window of neural coupling, this procedure was repeated for every lag within the COI pair until no significant difference of coupling indices between real pairs and nonpairs was observed anymore. Lastly, results were FDR-corrected for multiple comparisons.

Validation: Social Network Parameters. Correlation between coupling indices and SNI data were computed. Here, we found the complexity of the social network to be associated with the magnitude of neural coupling a subject displays during interaction ($r = 0.24$, $P = 0.04$). This relationship was not observed in nonpairs (all $r < 0.03$, all $P > 0.05$). Because the neural coupling index states a characteristic of the dyad, individual measures of social network complexity were averaged within each pair, forming dyadic social network complexity estimates (computed for all pairs for which both respective network data were available; $n = 70$ pairs or 35 pairs). For validation, mean social network complexity data were entered into a repeated measures ANOVA model, which included the neural coupling index as dependent variable, task block (A/B) as the within-subject factor, the mean social network complexity as independent variable, and within-pair SNI difference as a nuisance covariate.

ACKNOWLEDGMENTS. The authors thank Dr. Emanuel Schwarz for his valuable comments on the analysis and manuscript. E.B. is a PhD grant awardee of the SFB 636 International Graduate Program in Translational Neuroscience funded by the German Research Foundation (DFG). A.M.-L. gratefully acknowledges grant support by European Community's Seventh Framework Programme under Grant HEALTH-F2-2010-241909 (Project EU-GEI). A.M.-L., P.K., and C.S. gratefully acknowledge grant support by DFG (Clinical Research Unit 256, ME 1591/4-1). H.T. gratefully acknowledges grant support by the German Federal Ministry of Education and Research (BMBF 01GQ1102).

1. Noy L, Dekel E, Alon U (2011) The mirror game as a paradigm for studying the dynamics of two people improvising motion together. *Proc Natl Acad Sci USA* 108(52):20947–20952.
2. van der Wel RP, Knoblich G, Sebanz N (2011) Let the force be with us: Dyads exploit haptic coupling for coordination. *J Exp Psychol Hum Percept Perform* 37(5):1420–1431.
3. Sacheli LM, Tidoni E, Pavone EF, Aglioti SM, Candidi M (2013) Kinematics fingerprints of leader and follower role-taking during cooperative joint actions. *Exp Brain Res* 226(4):473–486.
4. Konvalinka I, Vuust P, Roepstorff A, Frith CD (2010) Follow you, follow me: Continuous mutual prediction and adaptation in joint tapping. *Q J Exp Psychol (Hove)* 63(11):2220–2230.
5. Pelphrey KA, Singerman JD, Allison T, McCarthy G (2003) Brain activation evoked by perception of gaze shifts: The influence of context. *Neuropsychologia* 41(2):156–170.
6. Schilbach L, et al. (2006) Being with virtual others: Neural correlates of social interaction. *Neuropsychologia* 44(5):718–730.
7. Anders S, Heinzle J, Weiskopf N, Ethofer T, Haynes JD (2011) Flow of affective information between communicating brains. *Neuroimage* 54(1):439–446.
8. Gordon I, Eilbott JA, Feldman R, Pelphrey KA, Vander Wyk BC (2013) Social, reward, and attention brain networks are involved when online bids for joint attention are met with congruent versus incongruent responses. *Soc Neurosci* 8(6):544–554.
9. Redcay E, Kleiner M, Saxe R (2012) Look at this: The neural correlates of initiating and responding to bids for joint attention. *Front Hum Neurosci* 6:169.
10. Montague PR, et al. (2002) Hyperscanning: Simultaneous fMRI during linked social interactions. *Neuroimage* 16(4):1159–1164.
11. King-Casas B, et al. (2005) Getting to know you: Reputation and trust in a two-person economic exchange. *Science* 308(5718):78–83.
12. Mundy P, Newell L (2007) Attention, joint attention, and social cognition. *Curr Dir Psychol Sci* 16(5):269–274.
13. Mundy P, Sullivan L, Mastergeorge AM (2009) A parallel and distributed-processing model of joint attention, social cognition and autism. *Autism Res* 2(1):2–21.
14. Charman T, et al. (2000) Testing joint attention, imitation, and play as infancy precursors to language and theory of mind. *Cogn Dev* 15(4):481–498.
15. Pelphrey KA, Shultz S, Hudac CM, Vander Wyk BC (2011) Research review: Constraining heterogeneity: The social brain and its development in autism spectrum disorder. *J Child Psychol Psychiatry* 52(6):631–644.
16. Calhoun VD, Adali T, Pearlson GD, Pekar JJ (2001) A method for making group inferences from functional MRI data using independent component analysis. *Hum Brain Mapp* 14(3):140–151.
17. Erhardt EB, et al. (2011) Comparison of multi-subject ICA methods for analysis of fMRI data. *Hum Brain Mapp* 32(12):2075–2095.
18. Allen EA, Erhardt EB, Wei Y, Eichele T, Calhoun VD (2012) Capturing inter-subject variability with group independent component analysis of fMRI data: A simulation study. *Neuroimage* 59(4):4141–4159.
19. Calhoun VD, Adalı T (2012) Multisubject independent component analysis of fMRI: A decade of intrinsic networks, default mode, and neurodiagnostic discovery. *IEEE Rev Biomed Eng* 5:60–73.
20. Stephens GJ, Silbert LJ, Hasson U (2010) Speaker–listener neural coupling underlies successful communication. *Proc Natl Acad Sci USA* 107(32):14425–14430.
21. Schippers MB, Roebroeck A, Renken R, Nanetti L, Keysers C (2010) Mapping the information flow from one brain to another during gestural communication. *Proc Natl Acad Sci USA* 107(20):9388–9393.
22. Cohen S, Doyle WJ, Skoner DP, Rabin BS, Gwaltney JM, Jr (1997) Social ties and susceptibility to the common cold. *JAMA* 277(24):1940–1944.
23. Bickart KC, Wright CI, Dautoff RJ, Dickerson BC, Barrett LF (2011) Amygdala volume and social network size in humans. *Nat Neurosci* 14(2):163–164.
24. Lewis PA, Rezaie R, Brown R, Roberts N, Dunbar RI (2011) Ventromedial prefrontal volume predicts understanding of others and social network size. *Neuroimage* 57(4):1624–1629.
25. Powell J, Lewis PA, Roberts N, Garcia-Finana M, Dunbar RI (2012) Orbital prefrontal cortex volume predicts social network size: An imaging study of individual differences in humans. *Proc Biol Sci* 279(1736):2157–2162.
26. Bickart KC, Hollenbeck MC, Barrett LF, Dickerson BC (2012) Intrinsic amygdala-cortical functional connectivity predicts social network size in humans. *J Neurosci* 32(42):14729–14741.
27. Decety J, Lamm C (2007) The role of the right temporoparietal junction in social interaction: How low-level computational processes contribute to meta-cognition. *Neuroscientist* 13(6):580–593.
28. Brothers L (1990) The social brain: A project for integrating primate behavior and neurophysiology in a new domain. *Concepts Neurosci* 1:27–51.
29. Meyer-Lindenberg A, Tost H (2012) Neural mechanisms of social risk for psychiatric disorders. *Nat Neurosci* 15(5):663–668.
30. Van Overwalle F (2009) Social cognition and the brain: A meta-analysis. *Hum Brain Mapp* 30(3):829–858.
31. Krall SC, et al. (2015) The role of the right temporoparietal junction in attention and social interaction as revealed by ALE meta-analysis. *Brain Struct Funct* 220(2):587–604.
32. Bzdok D, et al. (2013) Characterization of the temporo-parietal junction by combining data-driven parcellation, complementary connectivity analyses, and functional decoding. *Neuroimage* 81:381–392.
33. Schurz M, Radua J, Aichhorn M, Richlan F, Perner J (2014) Fractionating theory of mind: A meta-analysis of functional brain imaging studies. *Neurosci Biobehav Rev* 42:9–34.
34. Laube I, Kamphuis S, Dicke PW, Thier P (2011) Cortical processing of head- and eye-gaze cues guiding joint social attention. *Neuroimage* 54(2):1643–1653.
35. Schilbach L, et al. (2010) Minds made for sharing: Initiating joint attention recruits reward-related neurocircuitry. *J Cogn Neurosci* 22(12):2702–2715.
36. Saxe R (2006) Uniquely human social cognition. *Curr Opin Neurobiol* 16(2):235–239.
37. Williams JH, Waiter GD, Perra O, Perrett DI, Whiten A (2005) An fMRI study of joint attention experience. *Neuroimage* 25(1):133–140.
38. Sallet J, et al. (2011) Social network size affects neural circuits in macaques. *Science* 334(6056):697–700.
39. Takao H, Hayashi N, Ohtomo K (2011) Effect of scanner in longitudinal studies of brain volume changes. *J Magn Reson Imaging* 34(2):438–444.
40. Turner JA, et al. (2013) A multi-site resting state fMRI study on the amplitude of low frequency fluctuations in schizophrenia. *Front Neurosci* 7:137.
41. Jovicich J, et al. (2009) MRI-derived measurements of human subcortical, ventricular and intracranial brain volumes: Reliability effects of scan sessions, acquisition sequences, data analyses, scanner upgrade, scanner vendors and field strengths. *Neuroimage* 46(1):177–192.
42. Krasnow B, et al. (2003) Comparison of fMRI activation at 3 and 1.5 T during perceptual, cognitive, and affective processing. *Neuroimage* 18(4):813–826.
43. Friedman L, et al. (2008) Test-retest and between-site reliability in a multicenter fMRI study. *Hum Brain Mapp* 29(8):958–972.
44. Calhoun VD, Adali T (2006) Unmixing fMRI with independent component analysis. *IEEE Eng Med Biol Mag* 25(2):79–90.
45. Himberg J, Hyvärinen A, Esposito F (2004) Validating the independent components of neuroimaging time series via clustering and visualization. *Neuroimage* 22(3):1214–1222.